Supplement of Atmos. Chem. Phys., 23, 4123–4148, 2023
https://doi.org/10.5194/acp-23-4123-2023-supplement

Atmospheric Chemistry and Physics
Open Access
EGU

Supplement of

Observations of biogenic volatile organic compounds over a mixed temperate forest during the summer to autumn transition

Michael P. Vermeuel et al.

Correspondence to: Timothy H. Bertram (timothy.bertram@wisc.edu)

S1 GC collections and calibrations

S1.1 Routine field collections

Routinely, 2-3 sets of chromatograms were collected each day where each set consisted of a zero collection, two ambient sample collections, and a zero collection. The times of day chosen for each set were morning (~8:00 CDT), afternoon (~14:00 CDT), and evening (~21:00 CDT) to capture species with diurnal cycles that peak at different times in the day as well as those with speciation that may change throughout the day. For the evening collection, a calibration was performed, modifying the collection sequence to: zero, ambient sample, ambient sample, calibration, zero. Zeros were performed by overflowing the GC inlet with UZ air and a one-step calibration was performed through dilution of the VOC standard with UZ air. Multi-point calibrations of analytes were performed post-study to verify robustness of the measurement.

S1.2 Calibration of species not contained in calibration cylinder

To quantify the RetT of species not present in the field calibration standards permeation tubes were fabricated by addition of a liquid or solid standard to 3 mm ID PTFE tubing plugged at both ends with a PTFE rod and crimped at each end with stainless steel tubing (0.219" OD, 0.205" ID, 0.007" wall). The tubes were then heated to 40 ºC with 10 standard cubic centimeters (sccm) N2 flowing over it for 2 days to establish equilibrium and a consistent permeation rate. The 10 sccm analyte-containing flow was diluted with synthetic ZA. The dilution rate was determined by maintaining the MS analyte peak signal at 1% of the water dimer signal (m/Q 37.02841; $H_2O{\cdot}H_3O^+$).

S2 Cospectra, spectral corrections, and flux quality control

S2.1 Cospectra and cross-covariance

The averaged normalized co-spectra for the $C_{10}H_{17}^+$ (m/Q 137.1325; MT parent ion) and $C_5H_9^+$ (m/Q 69.06988; isoprene parent ion) signal for daytime periods of 10-19 CDT in winds of 2-2.5 m s^{-1} are shown in **Fig. S3a**. The spectral ogive (the cumulative area under the unnormalized co-spectra; dashed lines) generated for MT and isoprene (**Fig. S3b**) shows that >99.9% of the co-spectral area captured turbulent eddies with periods of 18 min or faster.

The sonic anemometer and the Vocus were separated by at most 45 m, creating a lag in time between w and C as the sampled air mass travels down the sampling tube. Since EC measurements require instantaneous values collocated in time, the cross-covariance, $f_X(t)$, of w and C from times 0 to 30 seconds was calculated for every flux period to determine the covariance at a prescribed lag time, t:

$$f_X(t) = \frac{1}{n-t}\sum_i^{n-t}(w_i - \bar{w})(C_{i+t} - \bar{C}) \quad \textbf{(ES1)}$$

The normalized cross-covariances of w and MT of multiple averaging periods and the mean of all cross-covariances is presented in **Fig. S3b**. The mean of the w-MT cross-covariance (t_{avg}) was 12 s. The calculated lag time is 11.6 s based on average volumetric flow rate pulled through the tube and the tube volume. Because a clear maximum in the

cross-covariance was observed in all flux periods, lag times from each individual 30-minute period for each species were calculated and used for quality control.

S2.2 Correction for attenuation of flux

Attenuation of flux due inlet damping, instrument response, and sensor separation was calculated from an empirical model (Horst, 1997) that requires an attenuation time constant, τ_c, also known as the response time. A correction factor is then calculated as:

$$\frac{F_m}{F} = \frac{1}{1+(2\pi n_m \tau_c U/z)^{\alpha}} \quad \textbf{(ES2)}$$

where F_m/F is the ratio of the measured flux to the unattenuated flux, U is wind speed, z is measurement height, and n_m and α are scaling factors for an unstable boundary layer taken as 0.085 and 7/8 respectively. The response time can be determined empirically by taking the ratio of the attenuated scalar normalized cospectra and the unattenuated cospectra from *w'T'* and is calculated as the frequency where the attenuated signal is reduced by $1/\sqrt{2}$. The τ_c for MT and isoprene was 0.32 seconds and for SQT and MTO was 0.64 seconds which would require correction factors of 2.3% and 4.1% for each time constant at the campaign daytime average windspeed of 2.3 m s^{-1}. Since these values were all lower than the flux uncertainty they were not applied.

S2.3 Flux quality control

Prior to Reynold's averaging of a flux period, C was despiked and detrended by subtraction of the linear fit of the signal time series. Winds were rotated based on the planar fit method (PFM), which is an assessment of the anemometer tilt with respect to long-term local streamlines (Wilczak et al., 2001). A plane was fit using 15-minute averaged sonic anemometer u, v, and w data from August-September 2020.

Flux periods were removed if any of the following conditions were true:

1. t_{avg} - 4 s > t_{max} > t_{avg} + 4 s, where t_{max} is the time point with a maximum in cross-covariance and t_{avg} is the campaign daytime average maximum lag time;
2. the mean flux value of five flux sub-periods differed from the value of the entire 30-minute flux period by more than 30% (i.e. stationarity test) (Foken & Wichura, 1996):

$$1 - \frac{\overline{\overline{w'C'}}_{sub-period}}{\overline{\overline{w'C'}}_{full\ period}} > 0.3 \quad \textbf{(ES3)}$$

3. the modeled and measured ratio in the standard deviation in wind and friction velocity (σ_w/u_*) differ by more than 30% (Foken et al., 2004), also known as integral turbulence characteristics (ITC_σ):

$$ITC_\sigma = \frac{(\frac{\sigma_w}{u_*})_{model} - (\frac{\sigma_w}{u_*})_{measured}}{(\frac{\sigma_w}{u_*})_{model}} \quad \textbf{(ES4)}$$

$$(\frac{\sigma_w}{u_*})_{model} = c_1(\frac{z}{L})^{c_2} \quad \textbf{(ES5)}$$

where z is the height above the surface, L is the Obukhov length, and c_1 and c_2 are coefficients of integral turbulence characteristics found in Foken et al. (2004).

S3 $C_5H_9^+$ signal correction for isoprene only

To correct the $C_5H_9^+$ signal to contain only isoprene, the contributions from *n*-aldehydes needed to be removed:

$$C_5H_9^+{}_{isoprene,RT} = C_5H_9^+{}_{total,RT} - C_5H_9^+{}_{n-ald,RT} \quad \textbf{(ES6)}.$$

This was performed by converting the parent *n*-aldehyde signals ($M_{n\text{-ald}}^+$) to their $C_5H_9^+$ signal ($C_5H_{9,n\text{-ald}}^+$) using the $C_5H_9^+/M^+$ ratios in GC peak areas of the aldehyde isomers (**Fig. S6**) and taking the sum.

$$C_5H_9^+{}_{n-ald,RT} = M^+{}_{C7ald,RT} \cdot \frac{C_5H_9^+{}_{C7ald,GC}}{M^+{}_{C7ald,GC}} + M^+{}_{C8ald,RT} \cdot \frac{C_5H_9^+{}_{C8ald,GC}}{M^+{}_{C8ald,GC}} + M^+{}_{C9ald,RT} \cdot \frac{C_5H_9^+{}_{C9ald,GC}}{M^+{}_{C9ald,GC}} \quad \textbf{(ES7)}$$

The error in this correction considers uncertainty in the *n*-aldehyde ratios as well as the calibration uncertainty in isoprene. The absolute uncertainty from $C_5H_9^+{}_{n-ald,RT}$ is calculated as the geometric sum of the standard deviation (σ) in the $C_5H_9^+/M^+$ ratios.

$$Unc._{C_5H_9^+{}_{n-ald,RT}} = \sqrt{(\sigma_{C7ald,ratio} \cdot M^+{}_{C7ald,GC})^2 + (\sigma_{C8ald,ratio} \cdot M^+{}_{C8ald,GC})^2 + (\sigma_{C9ald,ratio} \cdot M^+{}_{C9ald,GC})^2} \quad \textbf{(ES8)}$$

The relative uncertainty is then calculated as:

$$\%\ Unc_{[isoprene],RT} = 100\ x \sqrt{\left(\frac{Unc._{C_5H_9^+{}_{n-ald,RT}}}{C_5H_9^+{}_{isoprene,RT}}\right)^2 + \left(\frac{\sigma_{cal.factor,isoprene}}{cal.factor,isoprene}\right)^2} \quad \textbf{(ES9)}.$$

S4 Laboratory tests of *n*-aldehyde production internal to the measurement system

To determine the production of *n*-aldehyde internal to the GC, a post-field lab study was performed by sampling ZA containing 0-30 ppbv of O_3 through the GC-Vocus with and without the Na_2SO_3-filled oxidant trap. This experiment showed that a significant amount of *n*-aldehydes are produced from the sample trap at ambient O_3 (15-30 ppbv) in the absence of the oxidant trap (**Fig. S13**). An oxidant trap with unused Na_2SO_3 was then purged with N_2 and heated to 50 °C for 1 hour before being placed in-line with the GC-system to remove any compounds adhering to the Na_2SO_3 powder surface. Results from this experiment showed that the background signal from octanal is high when sampling without the oxidant trap in ambient O_3 and increases with increasing O_3. When replacing the trap there is a hysteresis in signal from the traps, with signals decaying with each run after replacing the oxidant trap material. Because of this, the first GC series performed after oxidant trap replacement were discarded from analysis to clear out contamination from this.

To check if *n*-aldehyde signal was from ozonolysis of compounds on the inlet surface, a post-field experiment was performed where varying concentrations of O_3 was added to the inlet manifold (**Fig. S14**). This experiment showed that inlet ozonolysis has a small effect on detected $C_5H_9^+$, with about 1.5 cps of $C_5H_9^+$ generated per ppbv O_3 added.

Supplementary Figures and Tables

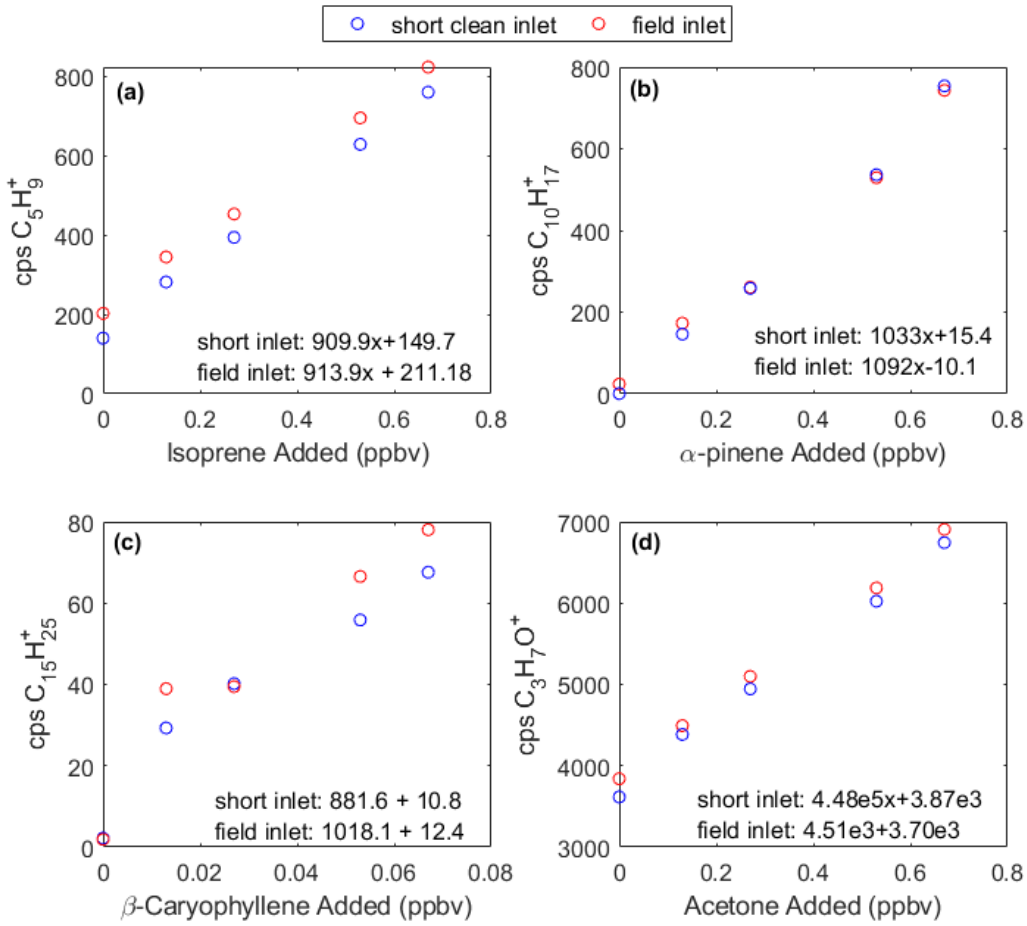

Figure S1: Comparison of calibration factors of isoprene (a), MT (b), SQT (c), and acetone (d) through the inlet used in the field (red circles) and a short, clean PFA line (blue circles).

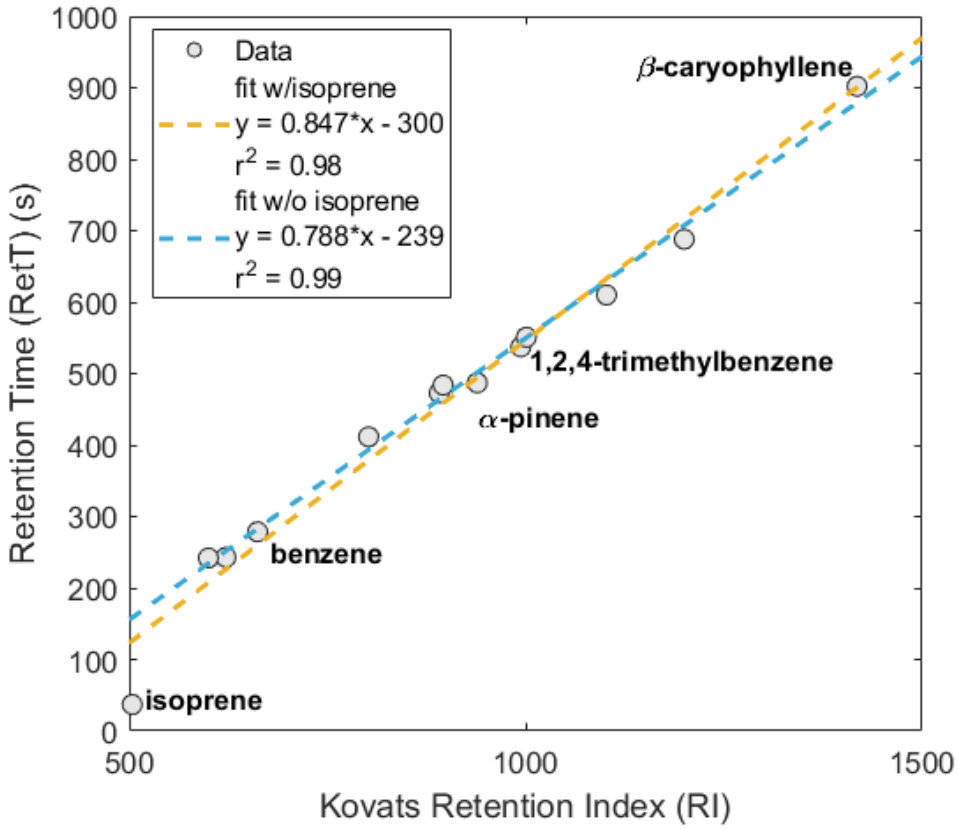

Figure S2: Determination of retention time (RT) using Kovats retention indices (RI). Compounds of matched RT and RI (grey circles) are fit using the isoprene data point (blue dash) and without (yellow dash). This study uses the fit without isoprene since the bulk of species quantified in this study have an RI>550 and early eluting species such as isoprene are at the lower mass limit of the capturing efficiency of the experimental adsorbent traps used.

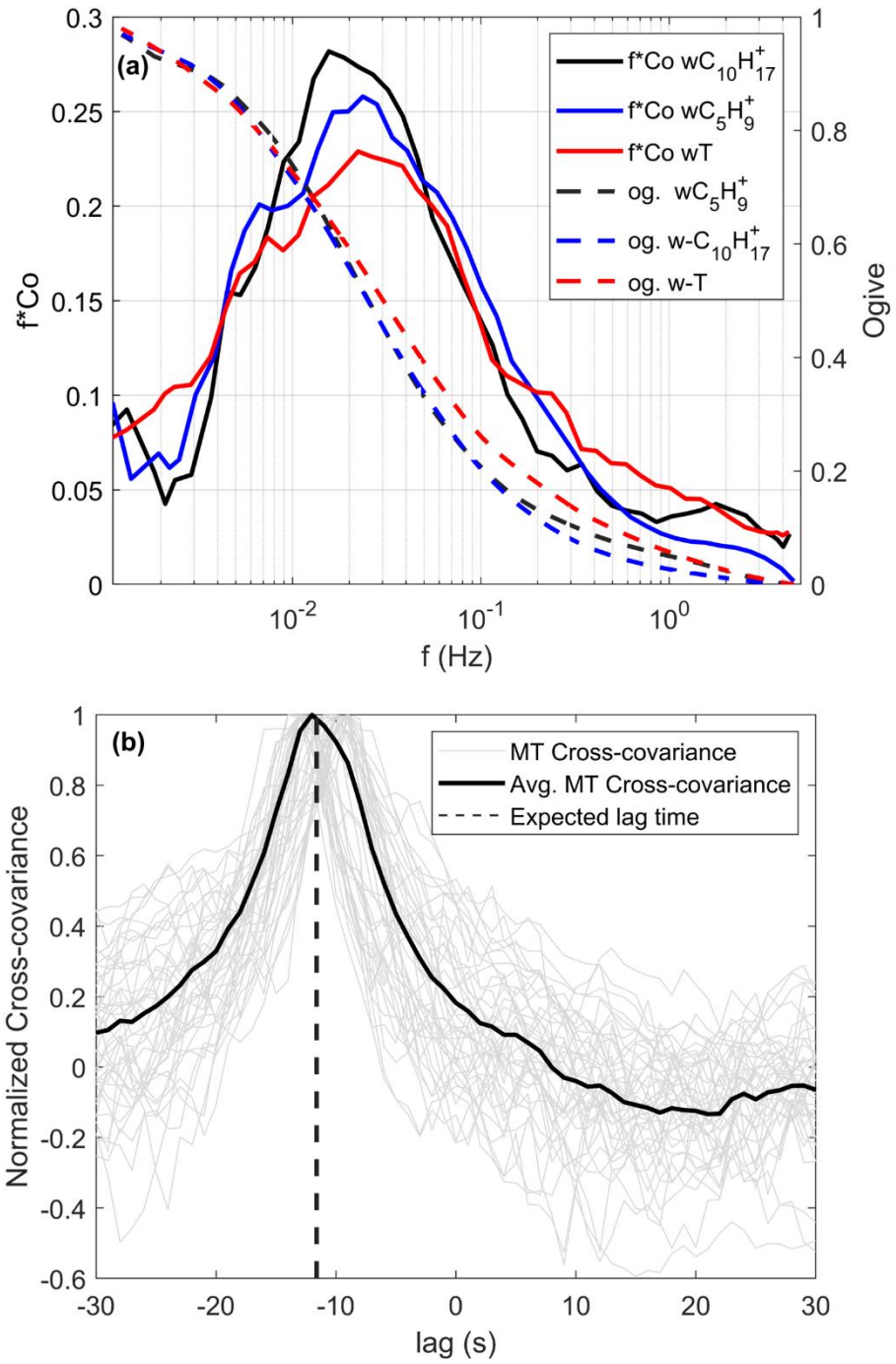

Figure S3: (a) frequency-normalized cospectra for *w*-*T* (red line) and *w*-MT (black line) along with their respective ogives (dashed lines). (b) normalized *w*-MT cross-covariances for individual daytime averaging periods the first two weeks of the study (grey lines) along with the average of those cross-covariances (black line) and the expected lag time (black dash).

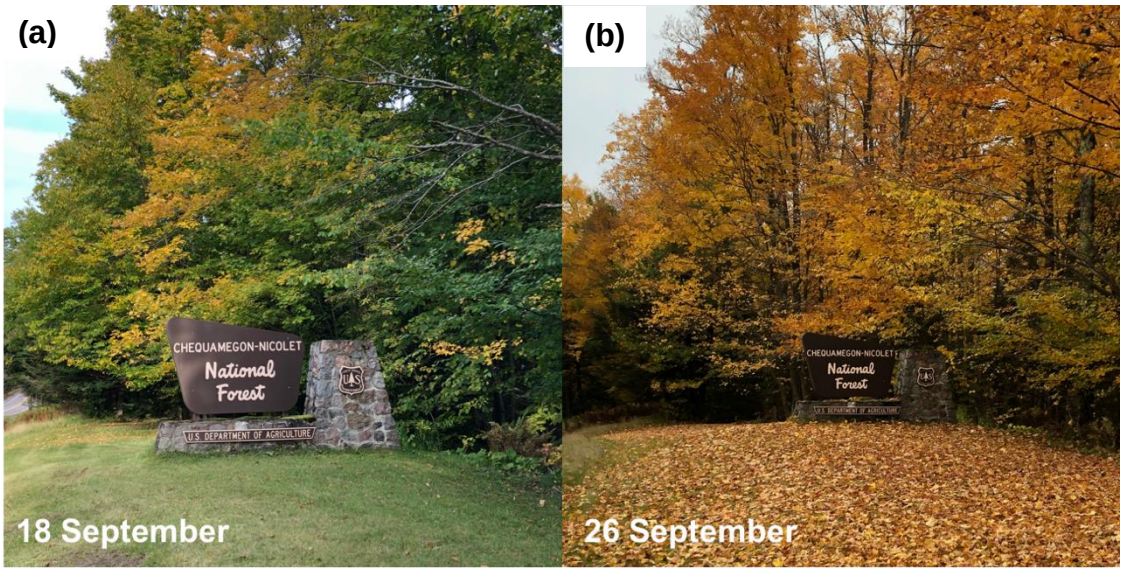

Figure S4: Images of a CNNF location on a. 18 September and b. 26 September 2020 at a location ~6 km from the WLEF-TV site. Leaves of this particular tree type began to age on 16 September, with leaves falling ~1 week later.

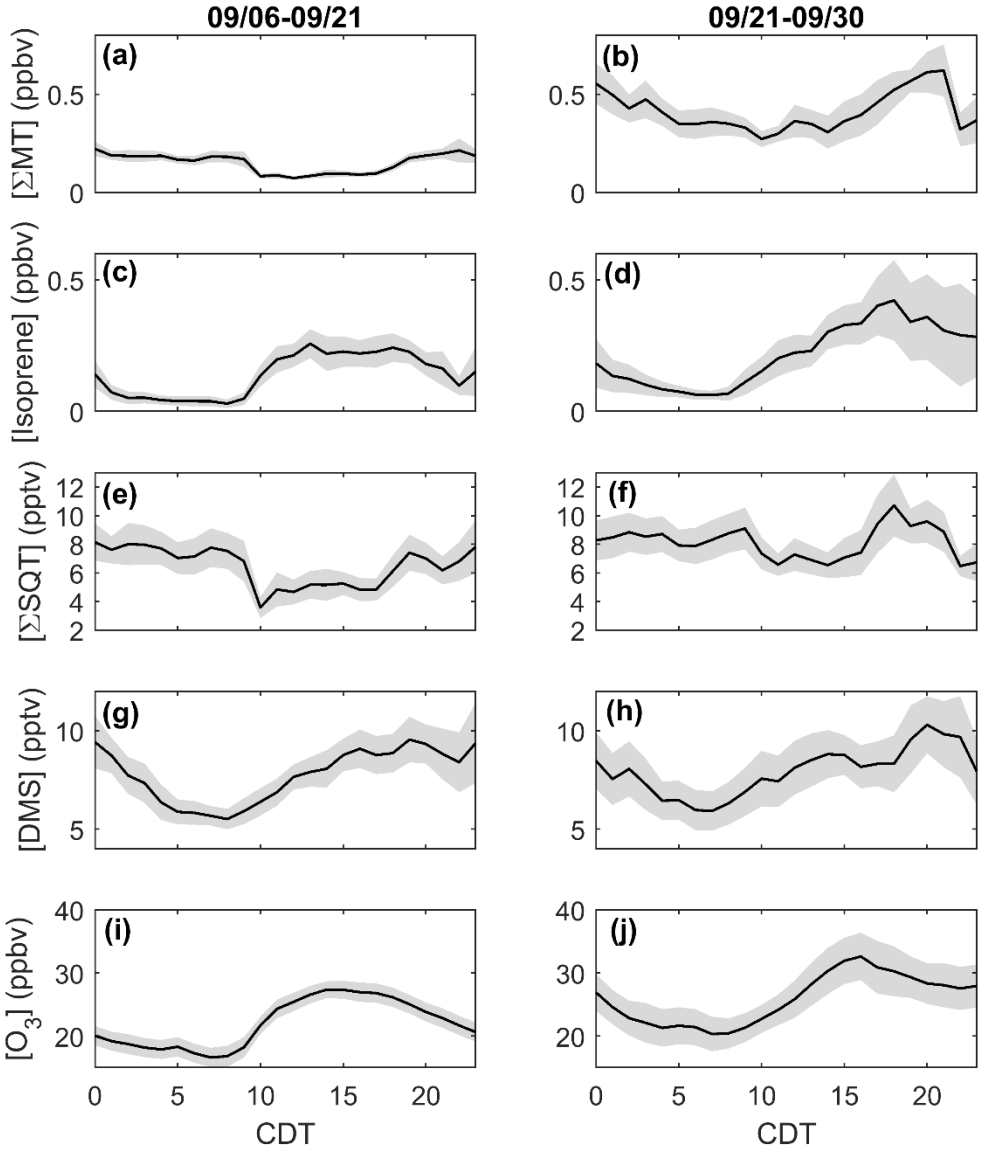

Figure S5: Diel profiles (mean, black line, and 95% confidence interval, shaded) for ∑MT (a + b), isoprene (c + d), ∑SQT (e + f), DMS (g + h), and O_3 (i + j) before and after 21 September.

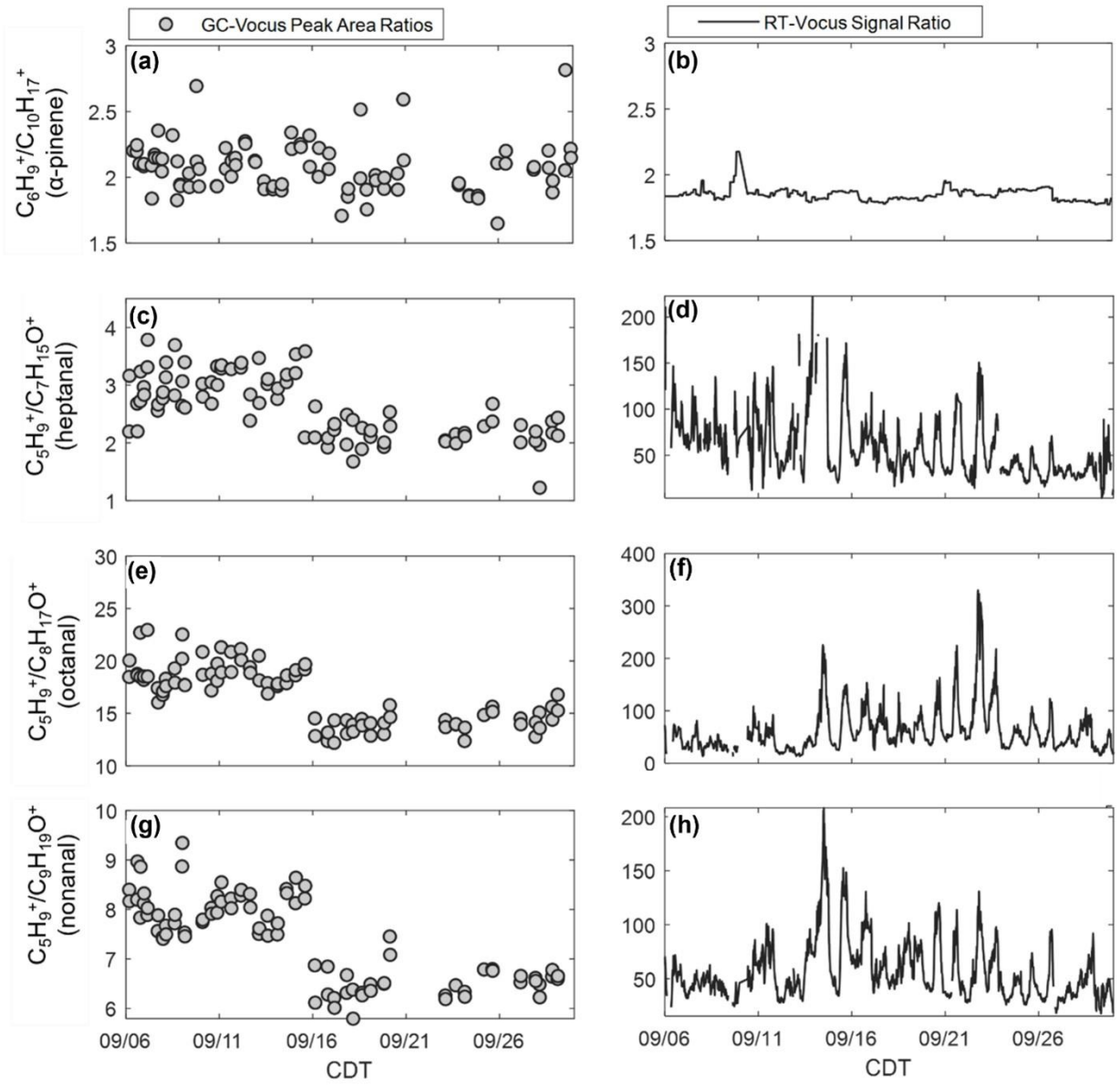

Figure S6: GC-Vocus peak area ratios of $C_6H_9^+$ and $C_{10}H_{17}^+$ (a) and RT-Vocus signal of $C_6H_9^+$ and $C_{10}H_{17}^+$ (b) are on average consistent between the two detection methods, validating the use of applying GC peak area ratios of fragment to parent ions to RT-Vocus signals. GC-Vocus peak area ratios of $C_5H_9^+$ and the *n*-aldehyde parent ions of heptanal, octanal, and nonanal do not agree, implying other ambient contributions to the $C_5H_9^+$ signal (c-h).

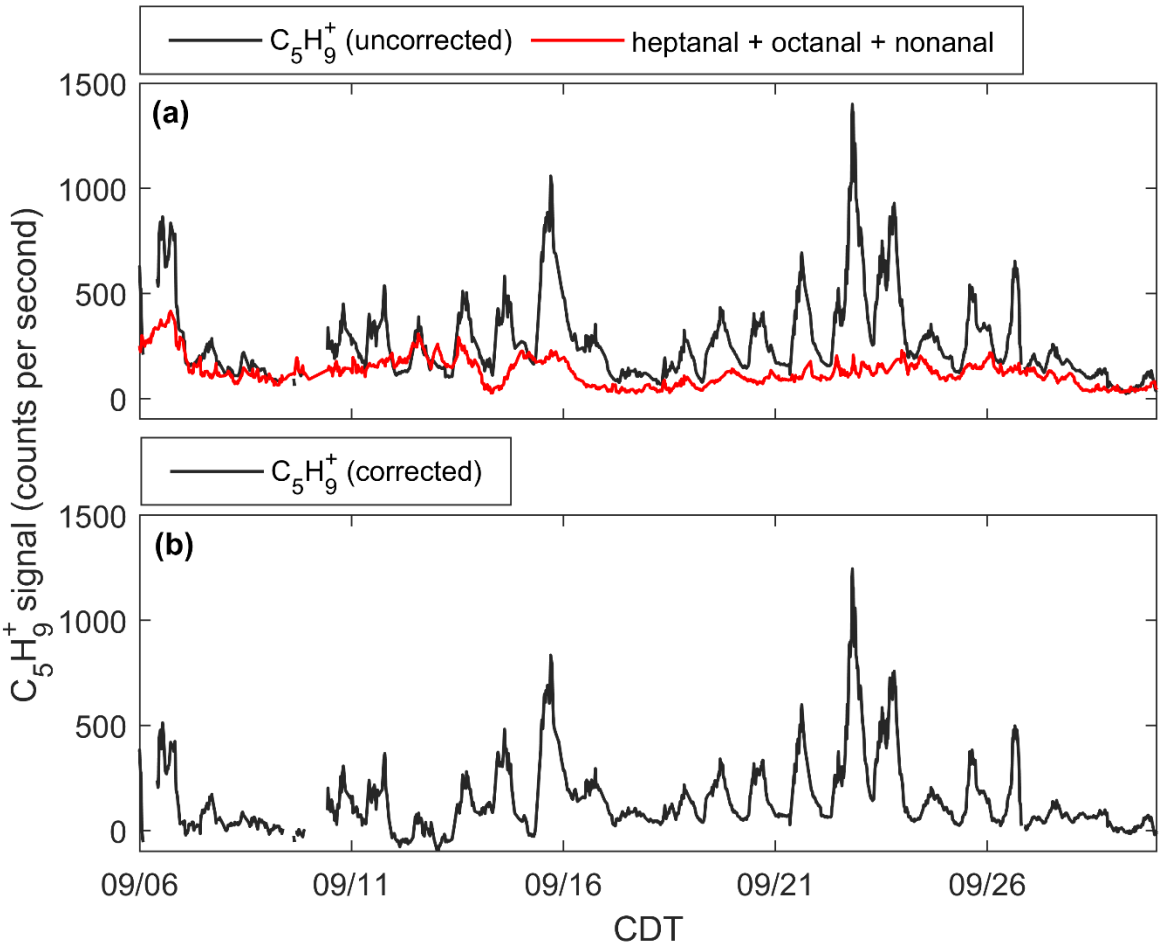

Figure S7: (a) uncorrected $C_5H_9^+$ (black line) signal and $C_5H_9^+$ signal from heptanal, octanal, and nonanal (red line). The *n*-aldehyde $C_5H_9^+$ signal (red line) was calculated by applying the $C_5H_9^+$:parent peak area ratios from Fig. S6 to the RT-Vocus parent signal. Subtraction of this *n*-aldehyde contribution provides the corrected $C_5H_9^+$ signal from isoprene only (b).

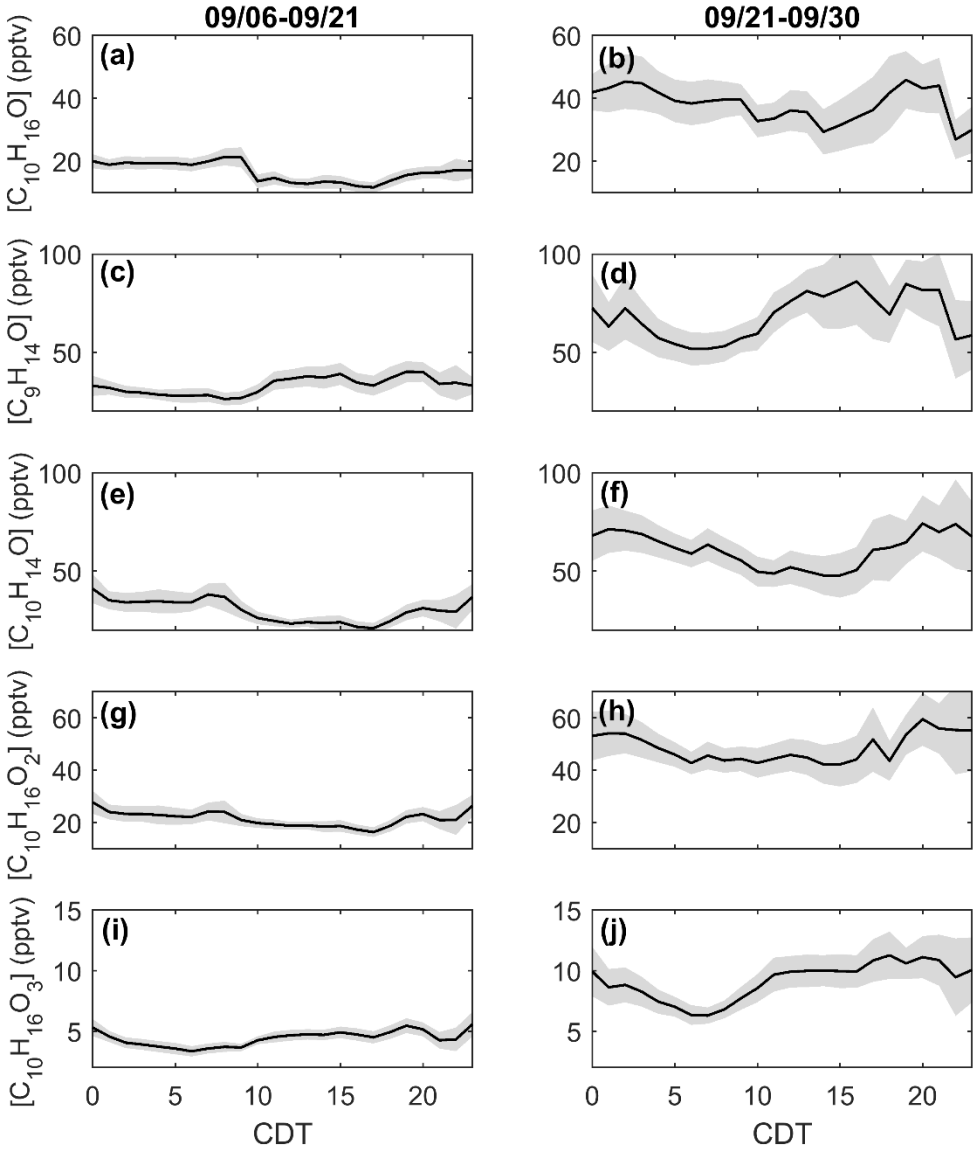

Figure S8: Diel profiles (mean, black line, and 95% confidence interval, shaded) for $C_{10}H_{16}O$ (a + b), $C_9H_{14}O$ (c + d), $C_{10}H_{14}O$ (e + f), $C_{10}H_{16}O_2$ (g + h), and $C_{10}H_{16}O_3$ (i + j) before and after 21 September.

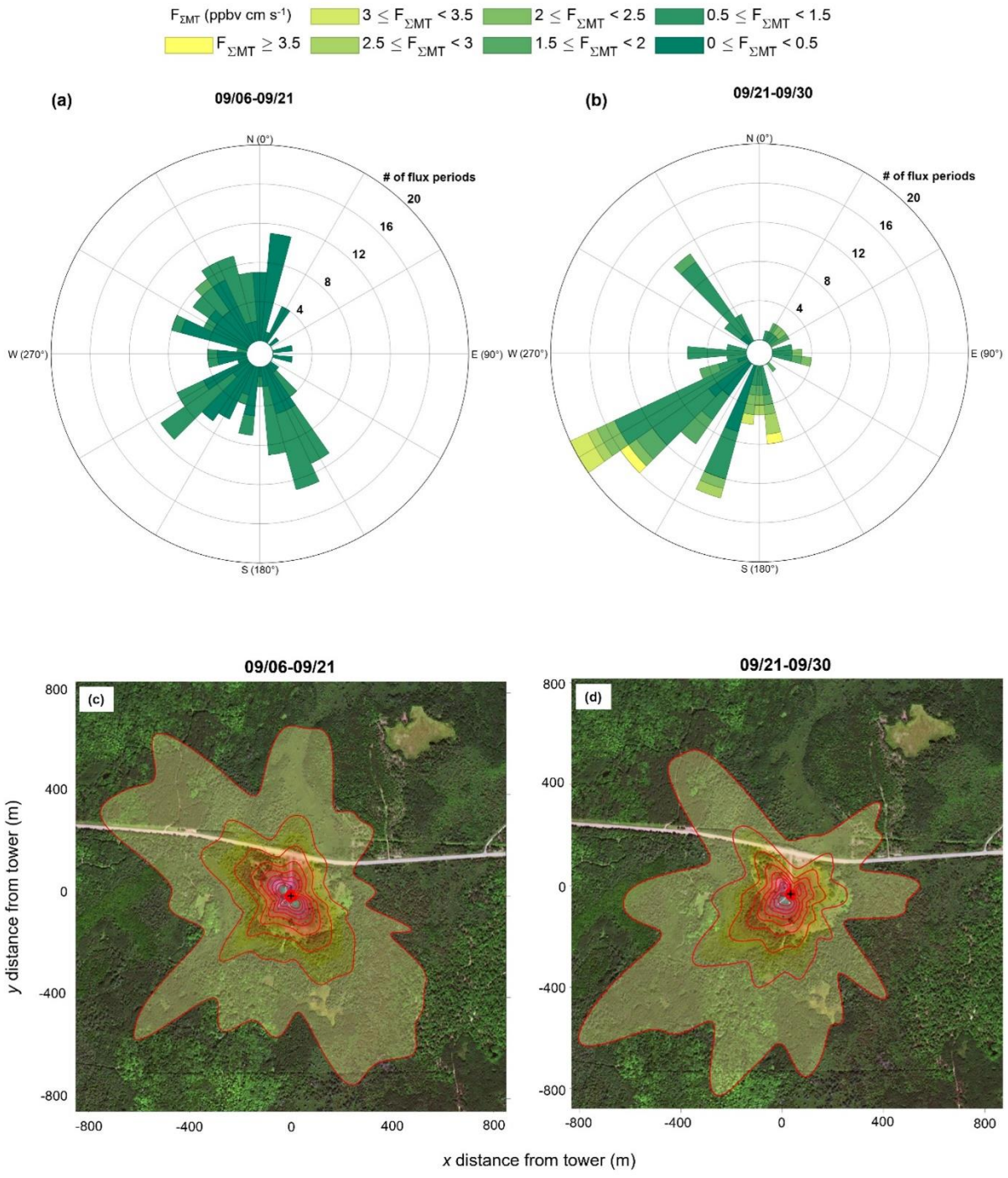

Figure S9: Flux sourcing of ∑MT based on wind direction before (a) and after (b) 21 September along with flux footprints before (c) and after (d) 21 September. Flux footprints were produced using the parameterization and code described in Kljun et al. (2015).

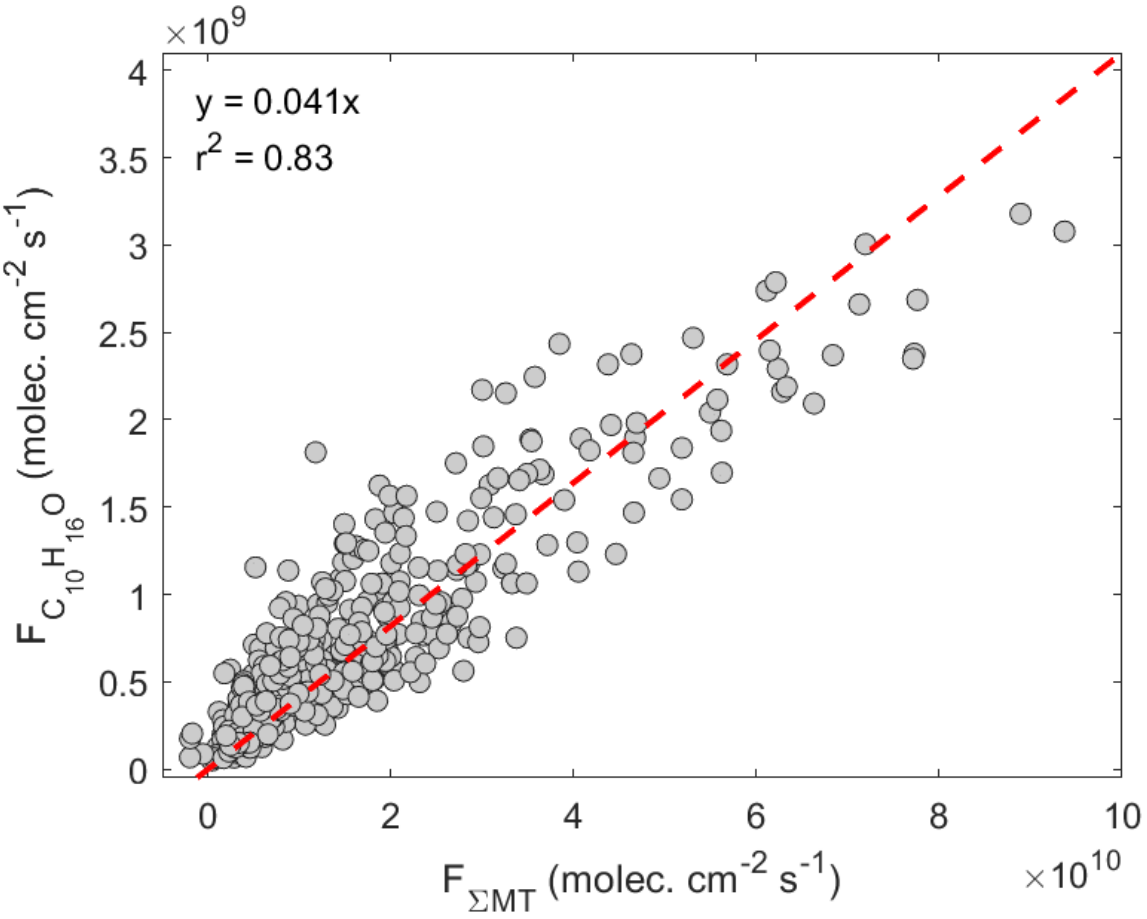

Figure S10: Regression of $F_{C_{10}H_{16}O}$ against $F_{\Sigma MT}$.

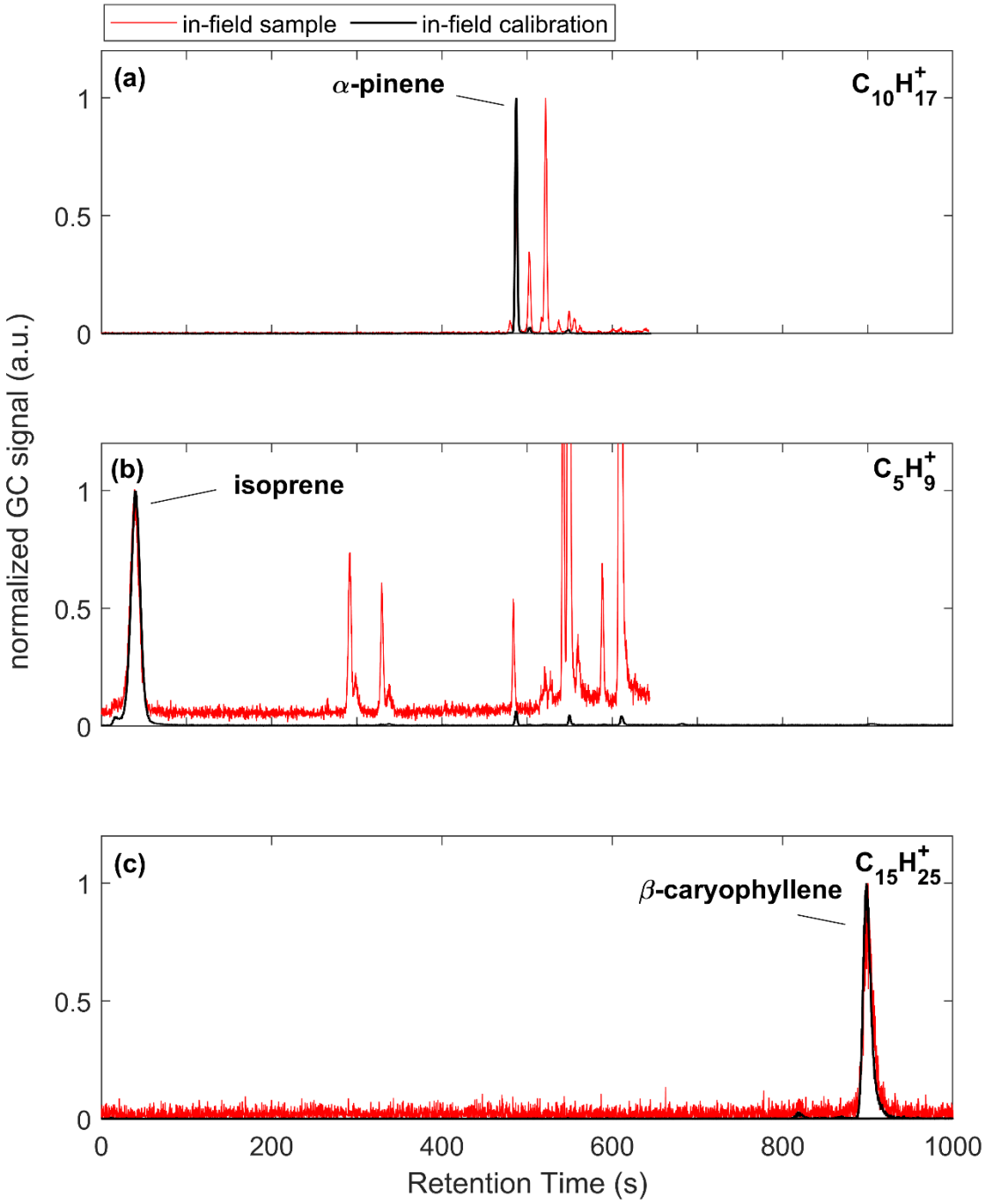

165

Figure S11: Sample (red) and calibration (black) chromatograms for (a) $C_{10}H_{17}^+$ and calibrated α-pinene, (b) $C_5H_9^+$ and calibrated isoprene, and (c) $C_{15}H_{25}^+$ and calibrated β-caryophyllene. Peak heights are normalized to the target peak.

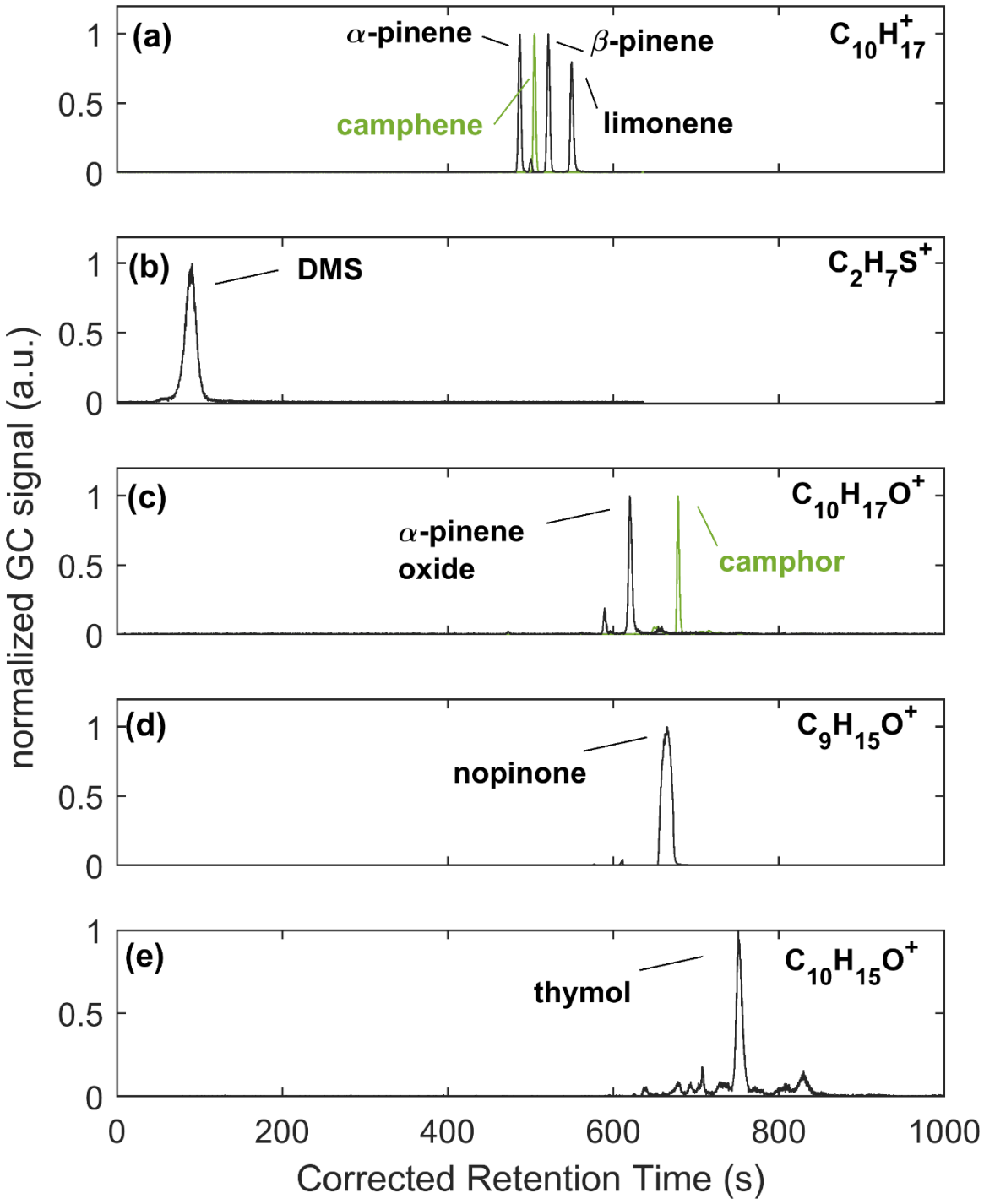

170 **Figure S12: Post-field calibration chromatograms of (a) $C_{10}H_{17}^+$, (b) $C_2H_7S^+$, (c) $C_{10}H_{17}O^+$, (d) $C_9H_{15}O^+$, and (e) $C_{10}H_{15}O^+$ species. The black and green lines indicate unique chromatogram collections.**

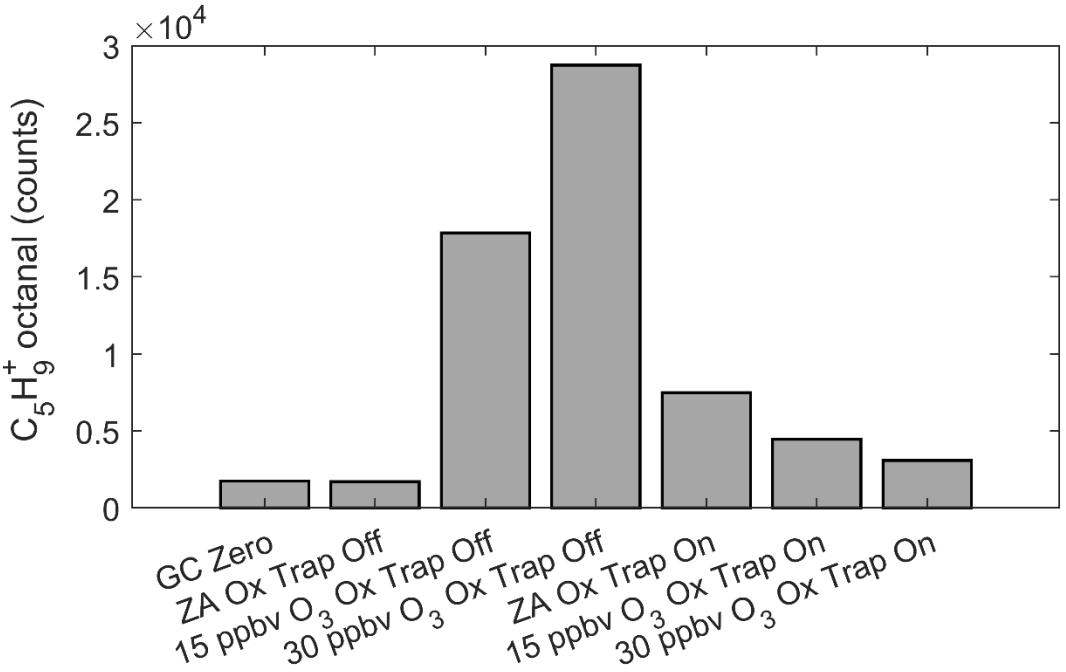

Figure S13: GC peak areas of octanal at the $C_5H_9^+$ signal. Each bar represents an individual collection. These collections included using the GC internal zero system (GC Zero), a sample collection of synthetic zero air with the oxidant trap removed (ZA Ox Off), and two sample collection with synthetic ZA and 15 or 30 ppbv O_3 (15/30 ppbv O_3 Ox Off). This process was repeated with the oxidant trap on (Ox On).

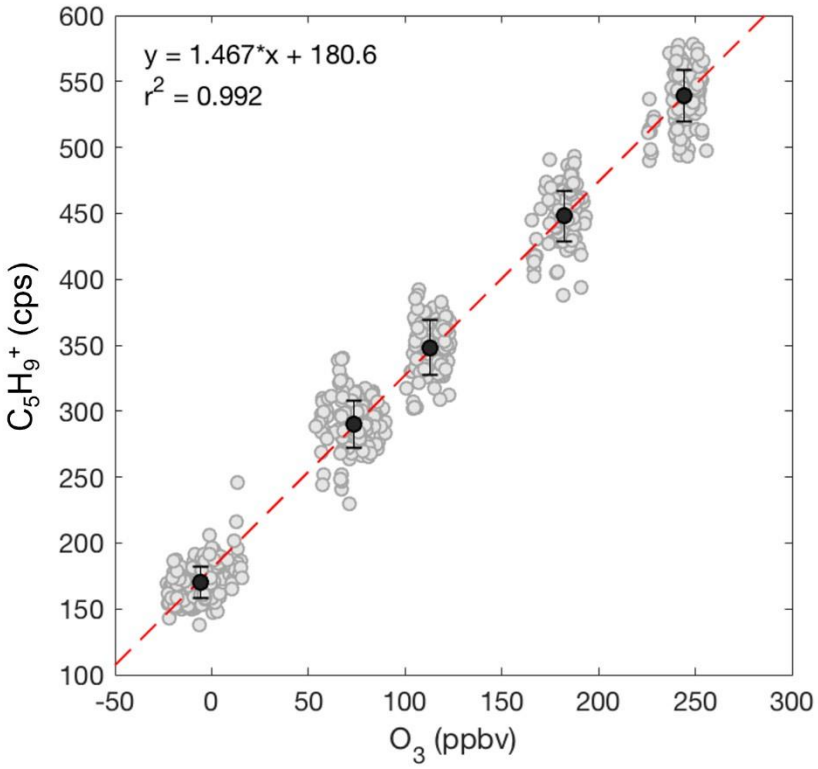

Figure S14: Addition of O_3 to field inlet shows a small response in $C_5H_9^+$ signal (~1.5 cps $C_5H_9^+$ ppbv O_3^{-1}).

185

190

195

200

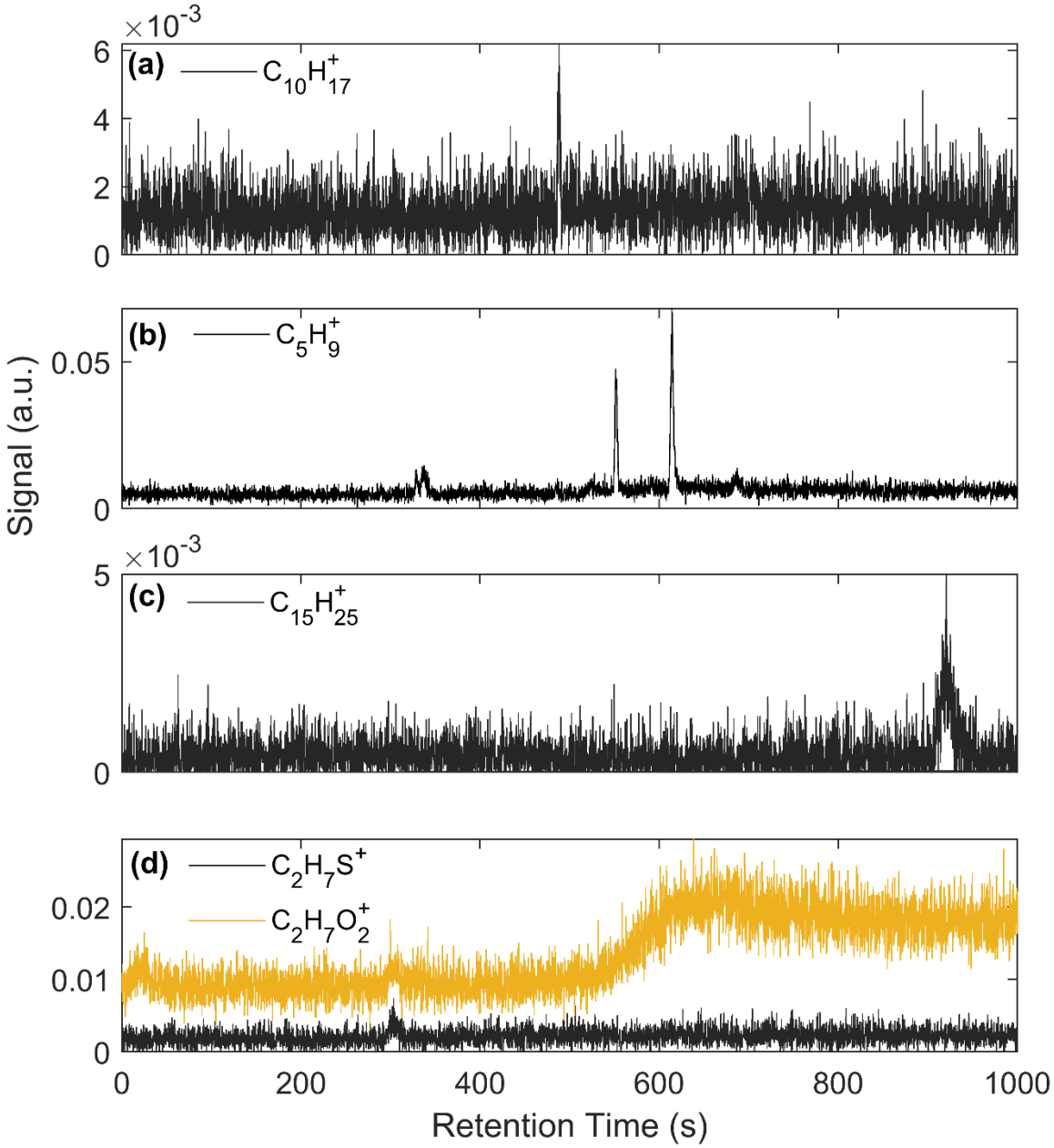

Figure S15: Background (zero) chromatograms for (a) $C_{10}H_{17}^+$, (b) $C_{10}H_{17}O^+$, (c) $C_5H_9^+$, (d) $C_{15}H_{25}^+$, and (e) $C_2H_7S^+$ and $C_2H_7O_2^+$.

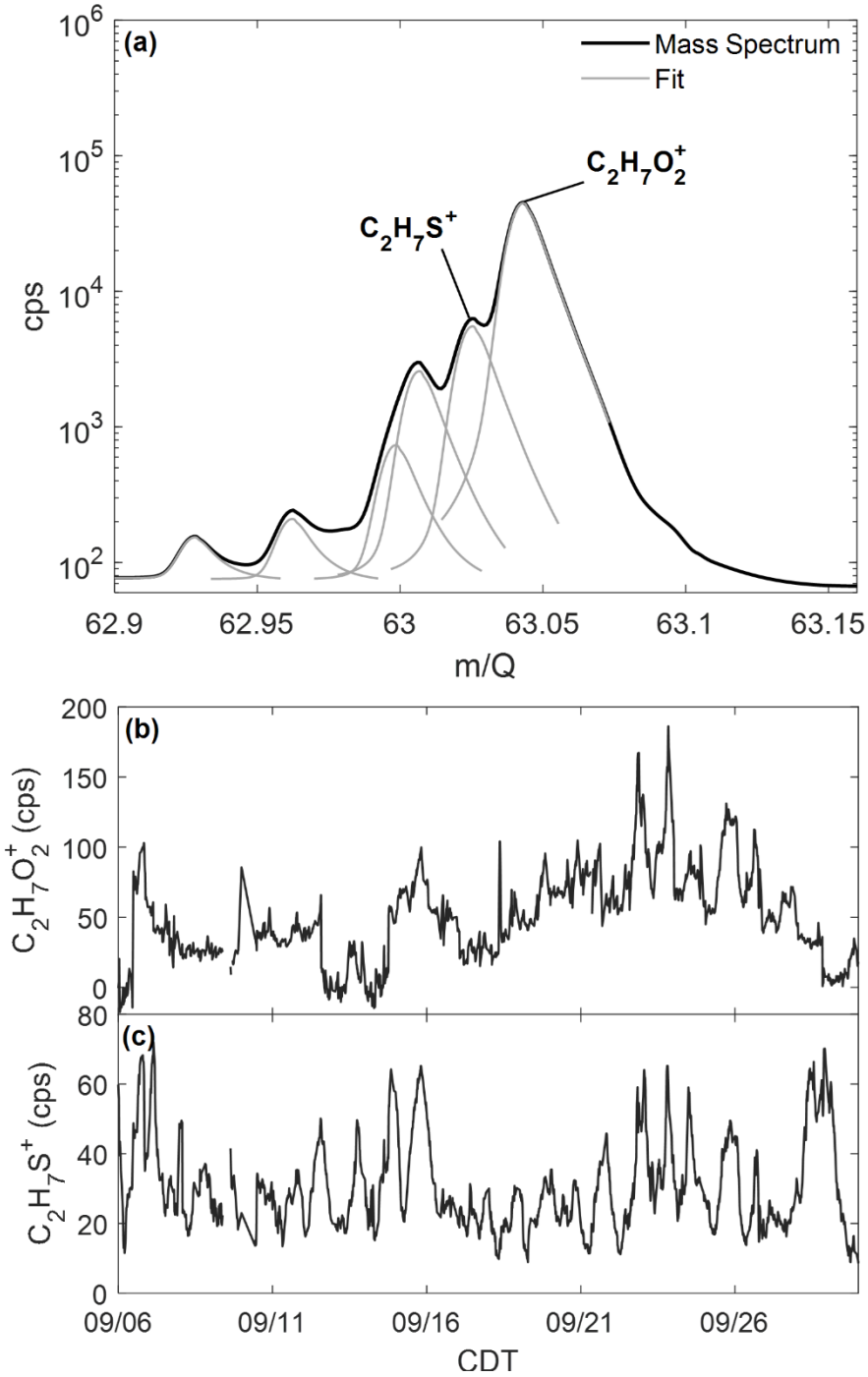

Figure S16: (a) Example mass spectra of the range m/*Q* 62.9-63.16 (black line) with fitted peaks (grey line). Time series of $C_2H_7O_2^+$ (b) and $C_2H_7S^+$ (c) show that these masses are individually resolved with distinct profiles.

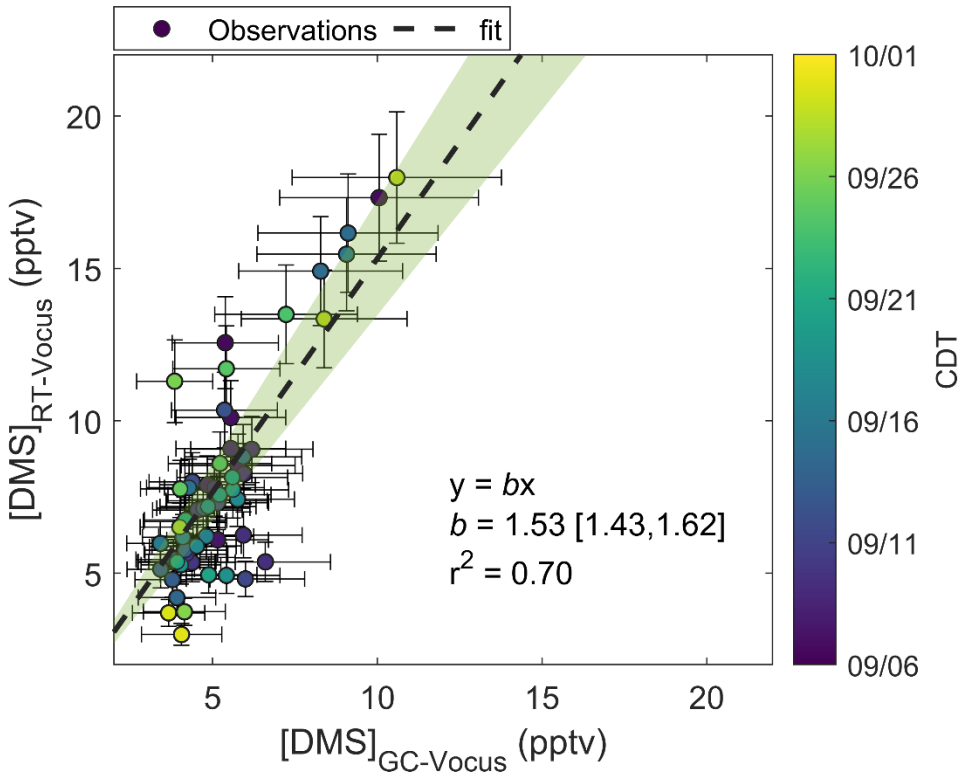

Figure S17: Regression of calibrated real time Vocus (RT-Vocus) and GC-Vocus DMS concentrations.

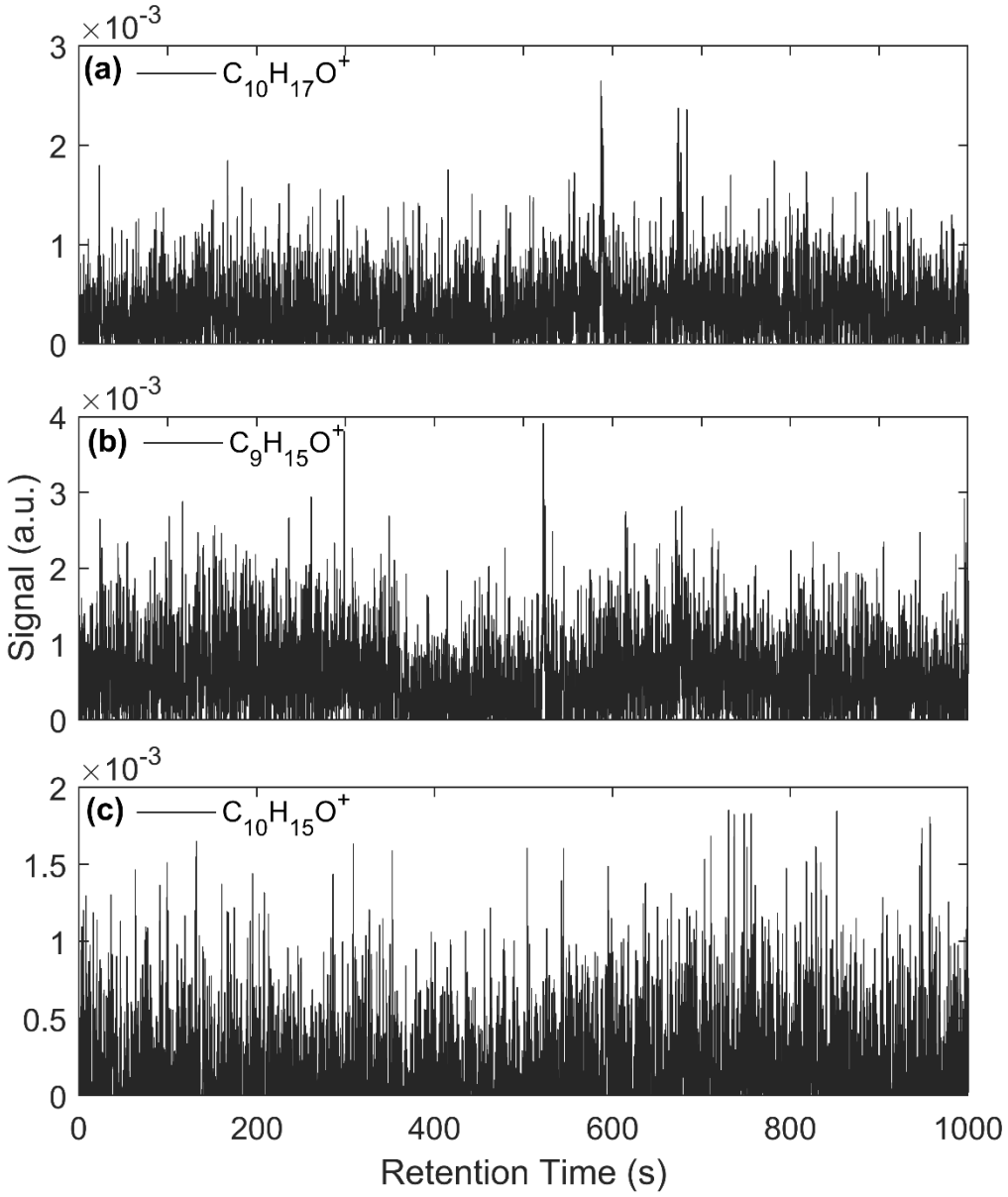

Figure S18: Background (zero) chromatograms for (a) $C_{10}H_{17}O^+$, (b) $C_9H_{15}O^+$, and (c) $C_{10}H_{15}O^+$.

230

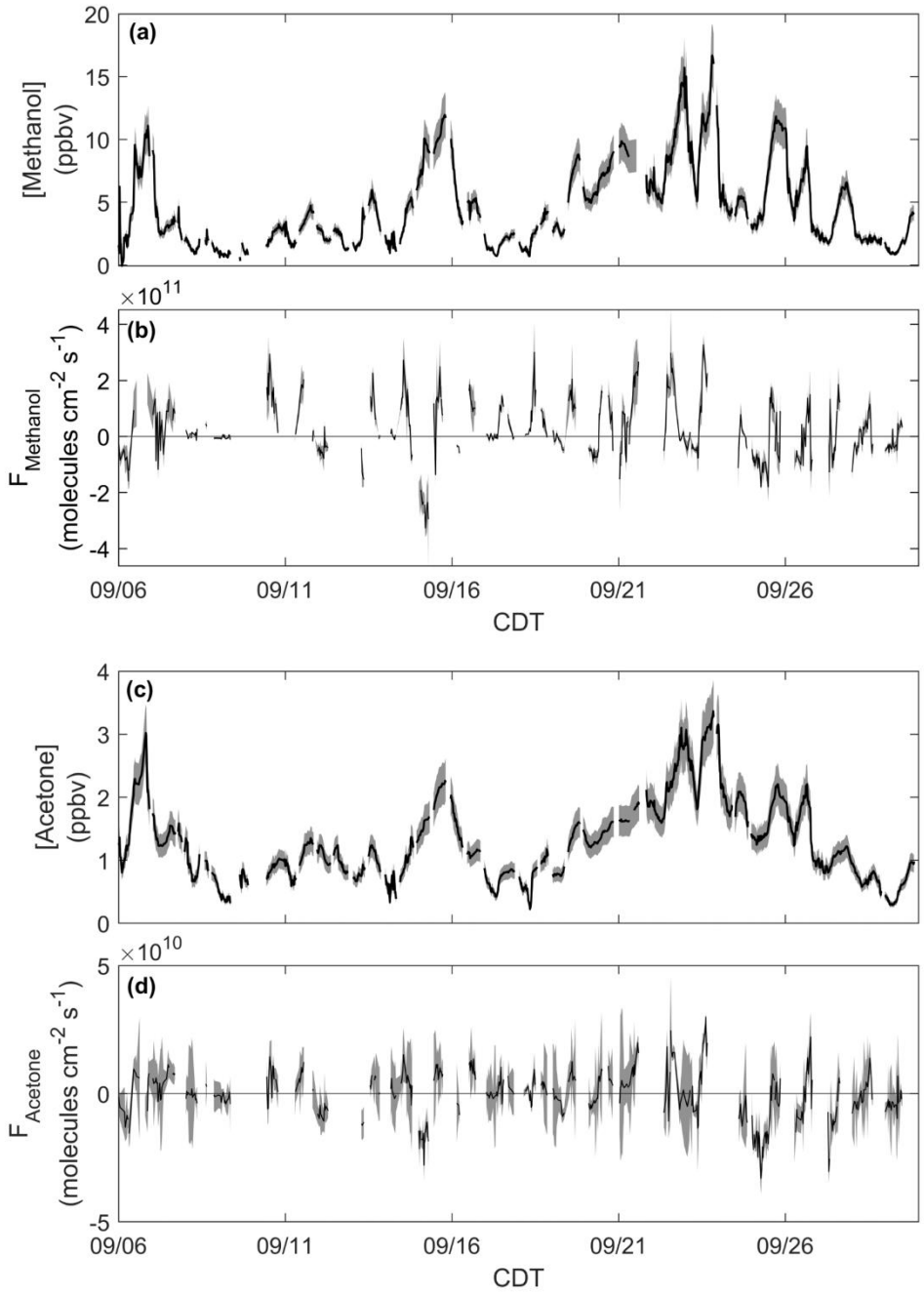

Figure S19: Methanol (a) concentrations and (b) fluxes. Acetone (c) concentrations and (d) fluxes. Shaded regions are measurement uncertainties.

Standard species	Concentration (ppbv)
Ethanol	1025
Acetonitrile	1034
Acetone	1020
Acrylonitrile	1017
Isoprene	1027
Methyl Vinyl Ketone	1024
Methyl Ethyl Ketone	1002
Benzene	1004
***o*-Xylene**	1007
α-pinene	986
1,2,4-Trimethylbenzene	975
Octamethylcyclotetrasiloxane (D4)	1000
Decamethylcyclopentasiloxane (D5)	1016
β-Caryophyllene	102

Table S1: Authentic NMVOC standards used for standard additions in the field.

Yield	α-pinene	β-pinene	camphene	isoprene	SQT
Y_{OH}	0.0044	0.0058	0.0058	0.0003	0.0058
Y_{O3}	0.034	0.0012	0.0012	0.0001	0.017
Y_{NO3}	0.001	0.001	0.001	0.001	0.001

Table S2: Yields (*Y*) of ELVOC from oxidation of select BVOC against OH and O_3 and NO_3.

Molecule	τ_{O3}	τ_{OH}	τ_{NO3}
α-pinene	3.9 hr	5.3 hr	4.5 hr
β-pinene	19 hr	3.5 hr	11 hr
camphene	1 month	5.4 hr	1.9 day
β-caryophyllene[a]	1.8 min	1.4 hr	1.5 hr
α-cedrene[a]	2.1 hr	4.0 hr	3.5 hr
β-farnesene	32.3 min	57.7 min	3.5 hr
isoprene	1.2 day	2.8 hr	1.7 day

Table S3: Model lifetimes of select terpenes against 30 ppbv O_3, 1 x 10^6 molecules cm^{-3} OH, and 1 x 10^7 molecules cm^{-3} NO_3, all at 298 K.

[a] not used in model but presented as a comparison of lifetimes for other potential SQTs.

	P_{HOM} $F_{MT,obs.}$	P_{HOM} $F_{MT,param.}$	P_{H2SO4} no SO_2	P_{H2SO4} w/SO_2
Full Study	5.9	2.5	0.023	5.9
Pre-09/21	4.4	2.7	0.025	6.5
Post-09/21	8.4	2.2	0.018	4.7

Table S4: Model solutions of P_{HOM} and P_{H2SO4}. All values are in units of 10^8 molecules cm^{-3} day^{-1}.

References

Foken, T. and Wichura, B.: Tools for quality assessment of surface-based flux measurements, Agric. For. Meteorol., 78, 83–105, https://doi.org/10.1016/0168-1923(95)02248-1, 1996.

Foken, T., Göckede, M., Mauder, M., Mahrt, L., Amiro, B. D., and Munger, J. W.: Post-field data quality control, Handb. micrometeorology a Guid. Surf. flux Meas. Anal., 29, 181–208, 2004.

Horst, T. W.: A simple formula for attenuation of eddy fluxes measured with first order response scalar sensors, Boundary-Layer Meteorol. 1997 822, 82, 219–233, https://doi.org/10.1023/A:1000229130034, 1997.

Wilczak, J. M., Oncley, S. P., and Stage, S. A.: Sonic anemometer tilt correction algorithms, Boundary-Layer Meteorol., 99, 127–150, https://doi.org/10.1023/A:1018966204465, 2001.